Carrier-density-wave transport property depth profilometry using spectroscopic photothermal radiometry of silicon wafers I: Theoretical aspects

Derrick Shaughnessy and Andreas Mandelis[a)]
Photothermal and Optoelectronic Diagnostics Laboratories, Department of Mechanical and Industrial Engineering, University of Toronto, Toronto M5S 3G8, Canada

(Received 9 October 2002; accepted 13 February 2003)

A theoretical model for the photothermal radiometric (PTR) signal from an indirect band-gap semiconductor excited by a laser of arbitrary wavelength is presented. The model has been used to investigate the spectral dependence of the sensitivity of the PTR signal to variations in the electronic transport parameters of the sample. Simulations show slight variations of the sensitivity to carrier lifetime and carrier diffusivity with excitation wavelength due to changes in the strength of the thermal contribution to the signal that are a result of changes in the difference between the photon energy and the band gap. The sensitivity of the PTR signal to changes in the front surface recombination velocity is shown to have a strong dependence on the excitation wavelength with the sensitivity decreasing as the absorption depth of the excitation source increases, allowing spectroscopic carrier-density-wave depth profilometric measurements. © *2003 American Institute of Physics.* [DOI: 10.1063/1.1565498]

I. INTRODUCTION

Several optical characterization techniques have been developed to determine the transport parameters of semiconductor wafers: Recombination lifetime, τ; carrier diffusivity or diffusion coefficient, D; front surface recombination velocity, S_1; and back surface recombination velocity, S_2. The lifetime that is generally measured during wafer characterization is an average of the carrier lifetimes throughout the optical absorption depth in the sample, which vary spatially due to the irregular distribution of defects and impurities that act as recombination centers. The large number of crystal defects at the surface results in a much shorter lifetime for carriers in the vicinity of the surface as compared to those in the bulk, and has led to the following definition of the effective lifetime[1]

$$\tau_{\text{eff}}^{-1} = \tau_{\text{bulk}}^{-1} + \tau_{\text{surface}}^{-1}. \tag{1}$$

Laser-induced photothermal radiometry (PTR) is a powerful characterization method that is capable of monitoring all four of the aforementioned transport parameters.[2] Investigation of the PTR signal dependence on the surface conditions for optical excitation over a range of absorption depths will lead to knowledge that could allow for depth profilometry of the carrier lifetime, and thus monitoring of contamination or implantation layers in silicon wafers, by varying the optical absorption depth and mathematically deconvoluting the overlayers.

Distinctly from purely optical methodologies, the photothermal radiometric technique relies on the collection of black body radiation from a sample that has been excited by an intensity-modulated or pulsed light source. For semiconductors, there are two sources of infrared radiative emissions. Following absorption of optical photons of energy greater than the band-gap energy, E_g, carriers will have kinetic energy $(h\nu - E_g)$ that is released through a rapid ($\sim 10^{-12}$ s) relaxation to the respective (conduction or valence) band edge. The short time scale of this process makes diffusion effects negligible[3,4] and results in a prompt thermal source with a distribution equivalent to the optical absorption profile. In indirect-gap semiconductors, and in particular in silicon, photoexcited carriers will further diffuse throughout the material, for an average time τ, before undergoing nonradiative recombination in the bulk and at the surface. This results in a delayed thermal source of magnitude E_g at the location of every recombining electron–hole pair. If the optical source is harmonically modulated at angular frequency ω, these thermal sources result in an induced harmonic temperature change of the material, $T(x,\omega)$: Along with the infrared emissions that exist at ambient temperature, as predicted by Planck's Law, there will be superposed the emissions due to the induced temperature fluctuations. It is assumed that the temperature fluctuation is small compared to the dc temperature of the material, so that a first-order approximation of the Stefan–Boltzmann Law gives the ac radiated power in an optically opaque media as

$$\Delta W(\omega) \approx 4\varepsilon\sigma T_0^3 \Delta T(\omega), \tag{2}$$

where σ is the Stefan–Boltzmann constant, ε is the surface emissivity, and T_0 is the ambient temperature.

The photoexcited carrier plasma itself is also a radiative infrared source. While infrared radiation lacks the energy required to excite carriers across the band gap and create electron–hole pairs, free carriers do weakly absorb infrared radiation in lower-energy intraband and band-to-defect transitions. Thus, the injection of free carriers will increase the

a)Electronic mail: mandelis@mie.utoronto.ca

infrared absorption of a semiconductor. According to Kirchoff's law of detailed balance, the rate of emission of black body radiation per wavelength interval for a body at thermal equilibrium with its surroundings is equal to the rate of absorption of incident radiation for the same wavelength interval.[5] Although the system is not in equilibrium when excess carriers are present, it has been shown that Kirchoff's law can still be applied to situations involving nonequilibrium carrier injection.[6] Accordingly, the existence of infrared absorption necessitates the existence of infrared emission and, introducing a modulated free carrier density, produces an ac infrared emission that is proportional to the depth integral of the free carrier density. This amounts to each recombining photoexcited carrier acting as a Planck emission radiator.[7]

The emitted radiation from both thermal and electronic sources is collected over a fixed solid angle and focused onto an appropriate infrared detector. In the case of a modulated source, the signal is monitored by a lock-in amplifier and the amplitude and phase of the PTR signal are fitted to an appropriate theory to determine the electronic transport parameters.

In this work, a rigorous theoretical framework for modeling the spectroscopic PTR signal from a semiconducting sample as a function of the optical absorption depth of the exciting radiation in the semiconductor is established. The sensitivity of the PTR signal to the transport parameters at various penetration depths is examined and the potential of spectroscopic PTR as a depth profilometric technique is established.

II. THEORETICAL MODEL

The following model is for the PTR signal from a semiconducting sample excited by a normally incident Gaussian-shaped laser beam with an axially symmetric intensity profile $I=I_0\exp(-r^2/w^2)$ and arbitrary wavelength. Here, w is the spotsize of the laser beam. The absorption of superband-gap photons results in a photon density that decays exponentially in the axial direction according to $e^{-\beta z}$, where $\beta=\beta(\lambda)$ is the absorption coefficient (the Beer–Lambert law). Despite the crystallographic structure of Si and other semiconductors, it is assumed that the material is isotropic, both thermally and electronically, so that for cylindrically symmetric optical excitation, the field will be independent of the azimuthal angle. The emitted infrared radiation is focused onto an appropriate detector of radius a.

The theory for PTR signal generation from an excited semiconductor is well established, but previous presentations have not been complete. A common assumption has been that the thermal component of the signal is negligible and the PTR amplitude is then fit to a simplified expression to obtain carrier recombination lifetime and in some instances surface recombination velocities.[8,9] Although it has been shown that the ratio of the contribution from the plasma component to the thermal component is larger for PTR than other photothermal detection techniques,[10] we have found that the thermal component superposed over the plasma contribution is too significant to be neglected altogether.[11] Furthermore, as discussed next, it is necessary to fit both the PTR amplitude and phase to satisfy uniqueness when attempting to determine the complete set of transport parameters. Recently, a complete theoretical model for the three-dimensional infrared PTR signal from strongly absorbed incident radiation has been presented.[12] In this work, that theoretical model is expanded to describe the three-dimensional PTR signal from a semiconductor undergoing low-level carrier injection from an optical source with an arbitrary absorption coefficient.

The transport of thermal energy and electronic carriers in an electronic material excited by a modulated source can be described by the temporal Fourier transforms of the heat conduction and Boltzmann transport equations, respectively. These coupled diffusion equations can be solved in Hankel space and the complete PTR signal can be determined. The thermal-wave field $T(r,z;\omega)$ is the solution to the following heat diffusion equation:[13]

$$\nabla^2 T(r,z;\omega)-\sigma_t^2(\omega)T(r,z;\omega) = -\frac{1}{k}[Q_t(r,z;\omega)+Q_r(r,z;\omega)], \tag{3}$$

where $\sigma_t^2=i\omega/\alpha$, α is the thermal diffusivity, k is the thermal conductivity, and Q_t and Q_r stand for the spatial thermal and carrier recombination sources of infrared radiation, respectively. The thermal boundary conditions are

$$-k\frac{d}{dz}T(r,z;\omega)\bigg|_{z=0}=S_1E_gN(r,0:\omega), \tag{4a}$$

$$k\frac{d}{dz}T(r,z;\omega)\bigg|_{z=L}=S_2E_gN(r,L:\omega), \tag{4b}$$

and the two thermal sources are

$$Q_t(r,z;\omega)=\frac{\beta P\eta(1-R)(h\nu-E_g)}{h\nu\pi w^2}e^{-(r/w)^2-\beta z}, \tag{5}$$

and

$$Q_r(r,z;\omega)=\frac{E_gN(r,z;\omega)}{\tau}, \tag{6}$$

where P is the power of the incident excitation source, η is the probability that an incident photon produces an electron–hole pair, R is the reflectivity, $h\nu$ is the photon energy, and E_g is the band-gap energy. The carrier-density-wave field $N(r,z;\omega)$ is the solution to the temporal Fourier transform of the transport equation:[13]

$$\nabla^2N(r,z;\omega)-\sigma_e^2N(r,z;\omega)=-\frac{G_e(r,z;\omega)}{D}, \tag{7}$$

where $\sigma_e^2=(1+i\omega\tau)/D\tau$. The boundary conditions for the carrier-density wave are

$$D\frac{d}{dz}N(r,z;\omega)\bigg|_{z=0}=S_1N(r,0:\omega), \tag{8a}$$

$$D\frac{d}{dz}N(r,z;\omega)\bigg|_{z=L}=-S_2N(r,L:\omega), \tag{8b}$$

and the injected carrier density is

$$G_e(r,z;\omega)=\frac{\beta P\eta(1-R)}{h\nu\pi w^2}e^{-(r/w)^2-\beta z}. \tag{9}$$

Taking advantage of the azimuthal independence of the fields, the two boundary value problems can be solved by taking Hankel transforms

$$\tilde{F}(q,z;\omega)=\int_0^\infty F(r,z;\omega)J_o(qr)rdr, \tag{10}$$

and solving the resulting one-dimensional ordinary differential equations using Green's function techniques.[13] The Hankel transforms of the transport equations are

$$\frac{d^2}{dz^2}\tilde{T}(q,z;\omega)-\xi_t^2\tilde{T}(q,z;\omega)+\frac{E_gN(q,z;\omega)}{k\tau}=-\frac{\beta\eta P(1-R)(h\nu-E_g)e^{-(q^2w^2/4)-\beta z}}{2\pi h\nu k}, \tag{11}$$

where

$$\xi_t^2=q^2+\sigma_t^2=q^2+\frac{i\omega}{\alpha}, \tag{12}$$

and

$$\frac{d^2}{dz^2}\tilde{N}(q,z;\omega)-\xi_e^2\tilde{N}(q,z;\omega)=-\frac{\beta\eta P(1-R)}{2\pi h\nu D}e^{-(q^2w^2/4)-\beta z}, \tag{13}$$

where

$$\xi_e^2=q^2+\sigma_e^2=q^2+\frac{1+i\omega\tau}{D\tau}. \tag{14}$$

Solving the carrier-density-wave field boundary value problem in Hankel space and integrating over the depth of the sample yields:

$$\tilde{N}(q;\omega)=\int_0^L\tilde{N}(q,z;\omega)dz=E(q)\left[\frac{(1-e^{-\xi_eL})}{\xi_e}(C_1(q)+C_2(q)e^{-\xi_el})-\frac{(1-e^{-\beta L})}{\beta}\right], \tag{15}$$

where

$$E(q)=\frac{\beta P\eta(1-R)e^{-q^2w^2/4}}{2h\nu\pi D(\beta^2-\xi_e^2)},$$

$$C_1(q)=A_1A_2\left[\frac{b_1-b_2e^{-(\beta-\xi_e)L}}{A_2-A_1e^{-2\xi_eL}}\right],$$

$$C_2(q)=\frac{b_1A_1-b_2A_2e^{-(\beta-\xi_e)L}}{A_2-A_1e^{-2\xi_eL}},$$

$$A_1\equiv\frac{D\xi_e-S_1}{D\xi_e+S_1},$$

$$A_2\equiv\frac{D\xi_e+S_2}{D\xi_e-S_2},$$

$$b_1\equiv\frac{D\beta+S_1}{D\xi_e-S_1},$$

$$b_2\equiv\frac{D\beta-S_2}{D\xi_e+S_2}.$$

The solution of the thermal-wave field in Hankel space, after integrating over the sample depth is:

$$\begin{aligned}\tilde{T}(q;\omega)&=\int_0^L\tilde{T}(q,z;\omega)dz\\&=B_1\frac{(1-e^{-\xi_tL})}{\xi_t}-B_2\frac{(1-e^{\xi_tL})}{\xi_t}+B_3\frac{(1-e^{-\xi_eL})}{\xi_e}+B_4\frac{(1-e^{-\xi_eL})}{\xi_e}e^{-\xi_eL}+B_5\frac{(1-e^{-\beta L})}{\beta},\end{aligned} \tag{16}$$

where

$$B_1\equiv\frac{h_1(q)-h_2(q)e^{-\xi_tL}}{1-e^{-2\xi_tL}},$$

$$B_2\equiv\frac{h_1(q)e^{-\xi_tL}-h_2(q)}{1-e^{-2\xi_tL}}e^{-\xi_tL},$$

$$B_3\equiv-\frac{E_gE(q)C_1(q)}{k\tau(\xi_e^2-\xi_t^2)},$$

$$B_4\equiv-\frac{E_gE(q)C_2(q)}{k\tau(\xi_e^2-\xi_t^2)},$$

$$B_5\equiv-\frac{H(q)-(E_g/\tau)E(q)}{k(\beta^2-\xi_t^2)},$$

$$H(q)=\frac{\beta P\eta(1-R)(h\nu-E_g)e^{-q^2w^2/4}}{2h\nu\pi D},$$

$$h_1(q)=\frac{S_1E_gE(q)}{k\xi_t}(C_1(q)+C_2(q)e^{-2\xi_eL}-1)-\frac{\xi_e}{\xi_t}(B_3-B_4e^{-2\xi_eL})-\frac{\beta}{\xi_t}B_5,$$

$$h_2(q)=-\frac{S_2E_gE(q)}{k\xi_t}(C_1(q)e^{-\xi_eL}+C_2(q)e^{-\xi_eL}-e^{-\beta L})-\frac{\xi_e}{\xi_t}(B_3-B_4)e^{-\xi_eL}-\frac{\beta}{\xi_t}B_5e^{-\beta L}.$$

Calculation of the PTR signal due to the combined infrared emissions of the thermal wave and the carrier-density wave must take into account the efficiency of the detector by integrating over the effective detector aperture.[12] Assuming a circular aperture of radius a, the PTR signal will be:

TABLE I. Optical properties of silicon for various wavelengths.

λ (nm)	n Ref. 15	k Ref. 15	R	$\beta=\frac{4\pi k}{\lambda}$ (m^{-1})	$1/\beta$ (m)
514	4.225	0.060	0.381	1.47×10^{6}	0.68×10^{-6}
710	3.773	0.0115	0.338	2.04×10^{5}	4.91×10^{-6}
810	3.685	0.006	0.328	9.31×10^{4}	10.74×10^{-6}
950	3.6	0.002 26	0.32	3.0×10^{4}	33.4×10^{-6}

$$S_{\mathrm{PTR}}=\frac{C_p}{\pi a}\int_0^\infty \tilde{N}(q;\omega)J_1(qa)dq + \frac{C_t}{\pi a}\int_0^\infty \tilde{T}(q;\omega)J_1(qa)dq, \tag{17}$$

where C_p and C_t are weighting factors to account for the relative strength of the two contributions (carrier wave and thermal wave) to the signal.

III. NUMERICAL SIMULATIONS

The theoretical model has been used to simulate the sensitivity of the PTR response in Si to the transport properties at several optical absorption depths over the range from 0.68 μm to 33.4 μm. The excitation wavelengths used for the simulations are shown in Table I with their corresponding optical absorption depths. Unless otherwise noted, the values for the electronic parameters used in the simulations are: $\tau=10^{-3}$ s, $D=25$ cm^2/s (corresponding to ambipolar diffusion), $S_1=300$ cm/s, $S_2=600$ cm/s, $C_p=1\times10^{-20}$ a.u., and $C_t=150$ a.u. A sample thickness of 675 μm (a typical Si wafer), a beam radius of 80 μm and an effective detector radius of 115 μm were used for all of the simulations. With the exception of the frequency-scan simulations, which are performed at constant incident power and account for variation in the reflection coefficient, the photon flux crossing the front surface is constant for the simulations at each wavelength. The results of the simulations are presented next to highlight several factors contributing to the uniqueness of PTR frequency-scan fits, the spectral dependence of the PTR signal over the range of physically relevant values for the transport parameters, and the experimental arrangement that should be used to best identify each transport parameter.

A well-known property of the amplitude of the PTR signal from an electronic material is the saturation at low frequencies with a characteristic bend that occurs at $\omega\tau\sim1$. The PTR amplitude at a frequency such that $\omega\tau>1$ is independent of lifetime (for reasons related to the electronic wave number that will be discussed next) and thus, at high frequencies, the slope of the PTR frequency-scan amplitude is independent of lifetime. At low frequencies ($\omega\tau<1$), the fast response of carriers with respect to the modulation period results in a saturated amplitude, with respect to frequency, that has a magnitude that increases with increasing lifetime due to the contribution of a larger number of carriers to the depth integral. Thus, in order to extract lifetimes from experiment it is important to ensure that frequencies below $\sim1/(2\pi\tau)$ are probed. At low lifetimes, the strength of the carrier-density-wave source is significantly decreased and the superposition of the thermal signal with the plasma signal can result in a PTR amplitude that is not saturated at low frequency but has a negative slope with a magnitude dependent on the relative strength of the thermal component. The presence of a strong thermal component also results in an increase in the phase lag for the low frequencies as the lifetime decreases.

The prevalence of the thermal component has ramifications on the spectral dependencies of the PTR sensitivity to changes in the carrier lifetime. While the sensitivity of the PTR signal component from the carrier-density wave to the carrier lifetime shows no variation with changing absorption depth, the strength of the thermal component at low frequencies and low lifetimes does introduce a spectral dependence of the signal to lifetime. For a constant photon flux across the surface, the shorter wavelengths deposit more energy to the lattice via the rapid thermalization of excited carriers, proportional to the difference between the photon energy and the band-gap energy, and thus exhibit higher amplitudes and larger phase lags as a result of the larger thermal component. Simulations using the aforementioned transport properties show that at low frequencies the difference in the strength of the thermal component is significant: Comparing the 514 nm and 950 nm results at 100 Hz reveals a difference of 19% in amplitude and 3.7° in phase for a lifetime of 1 μs but once the lifetime reaches 127 μs, there is a difference of only 1.8% in amplitude and 1.2° in phase. At 5 kHz, there are essentially no spectroscopic features to the amplitude while the phase exhibits a slight separation for lifetimes below approximately 20 μs.

A similar simulation for the dependence of the PTR signal on the diffusion coefficient (or diffusivity) shows that the amplitude decreases at all frequencies as the diffusivity increases. This is a result of increasing lateral transport that decreases the carrier density within the field of view of the detector. For frequencies such that $\omega\tau\gg1$, the electronic wave number is dependent solely on the diffusivity, $\sigma_e\approx(i\omega/D)^{1/2}$, resulting in an increased sensitivity of the PTR phase to diffusivity at higher frequencies. The difference in the effects of a variation of lifetime and diffusivity on the high-frequency response ensures a unique fit with respect to these two parameters. However, the complicated dependence of the signal on the other transport parameters present in Eq. (15) does not allow the diffusivity to be easily extracted directly from the slope of the amplitude or phase.

Examination of the spectral dependence of the PTR sensitivity to the diffusion coefficient shows resolved amplitude and phase as the diffusivity decreases. A similar simulation with the front surface recombination velocity (FSRV) equal to zero shows no such spectral dependence and thus identifies the source of the diverging signals with decreasing diffusivity. The more strongly absorbed wavelengths deposit carriers much closer to the surface than the longer wavelengths and as the diffusivity decreases the surface recombination becomes more prevalent, suppressing the amplitude of the shorter wavelengths. However, it should be noted that at literature values for the carrier diffusion coefficient (a review by Rodriguez *et al.*[2] found values of $D_n\sim35$ cm^2/s and $D_p\sim12.5$ cm^2/s), any spectral separation of the PTR response

due to this phenomenon is minimal and would be difficult to resolve experimentally.

Of greater significance in this range of diffusivities is the relative increase and decrease, respectively, of the low-frequency amplitudes and phase as the excitation wavelength decreases. At higher diffusivities, the relative strength of the thermal component of the signal with respect to the electronic contribution increases as carriers leave the field of view of the detector. The shorter the wavelength, the greater the difference between the photon energy and the band-gap energy, and thus the larger the thermal contribution from the rapid transfer of energy to the lattice via phonons before carrier diffusion occurs. This results in shorter wavelengths having a slightly lower sensitivity to the diffusion coefficient for high diffusivity values. However, for $D=35\ \mathrm{cm}^2/\mathrm{s}$ at 100 Hz, the amplitude difference and phase difference between the 514 nm and 950 nm values are 3.2% and 1.2°, respectively. Again, any spectroscopic features introduced by this phenomenon would be difficult to resolve experimentally. A decrease in the thermal weighting factor eliminates this spectral dependence and results in the response from the various excitation wavelengths converging as the diffusivity increases.

Although the diffusion length of an excited carrier is related to the diffusivity by the relation $L_D=(D\tau)^{1/2}$, for modulated injected carriers, the distance traveled by a carrier is described by the diffusion length of the carrier-density wave, $L_{\mathrm{ac}}(\omega)=L_D/(1+i\omega\tau)^{1/2}$. If this ac diffusion length is longer than the wafer thickness, carriers are able to travel to the back surface and the back surface recombination velocity (BSRV) will affect the PTR signal. Neither the amplitude nor the phase is sensitive to the BSRV at high frequencies, where the ac diffusion length becomes short relative to the sample thickness. At low frequencies, such that $\omega\tau<1$, the ac diffusion length is very weakly dependent on frequency thus any contribution to the PTR signal due to the back surface recombination is essentially constant with respect to frequency. For sufficiently long ac diffusion lengths, increased BSRV results in higher recombination that decreases the carrier density and thus lowers the low-frequency saturation level of the amplitude curve.

The PTR phase is not sensitive to changes in the BSRV at low frequencies because the signal is still dominated by the forward diffusing carrier-density-wave component and the relatively few carriers reflected from the back surface are not significantly phase shifted with respect to the forward moving carrier wave. However, as the frequency increases the phase centroid (determined by the weighted phase shifts of the reflected carrier wave and the forward carrier wave) becomes significant and we see a change in the phase as the BSRV increases. This appears as an overall phase lag, as expected from the enhanced importance of the reflected carrier-density-wave contribution. Finally at high frequencies, the ac diffusion length is too short for the critically damped carrier wave to reach the back surface and the quality of the back surface becomes irrelevant. This amplitude-phase response is unique to the variations in BSRV and allows for the possibility of scanning the sample at an intermediate frequency and utilizing variations in phase with no corresponding variation in amplitude to map the BSRV.

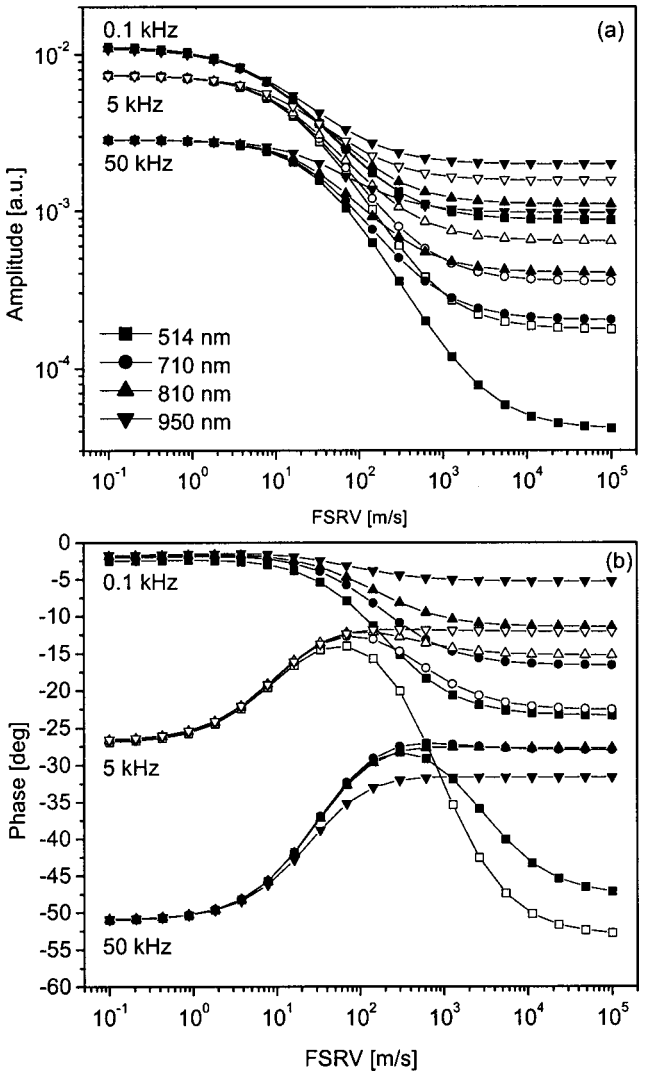

FIG. 1. Simulated PTR amplitude (a) and phase (b) as a function of FSRV.

The variation of the PTR signal with small changes in the BSRV for a high-quality surface (i.e., a surface with low carrier recombination velocity) is similar to that resulting from small variations in the recombination lifetime and suggests that it may be possible to compensate for changes among these two parameters for a high-quality surface, allowing for the possibility that only a range for the BSRV can be established. The simulations show little or no spectral dependence for the sensitivity to the BSRV because the increase in penetration depth over the selected wavelength range chosen in this study is relatively short compared to the sample thickness.

The PTR amplitude and phase are both sensitive to the FSRV over the entire frequency range of interest (Fig. 1) with higher sensitivity at higher frequencies. The shorter ac diffusion length at higher frequencies keeps the injected carriers closer to the surface and thus increases the probability of interaction with the recombination centers at the surface. Higher recombination rates due to high FSRV values lower the carrier density and result in lower amplitudes. Excitation sources with smaller absorption coefficients exhibit a smaller

decrease in amplitude for a given change in FSRV since fewer carriers are deposited in the vicinity of the surface.

The PTR phase lag initially decreases with increasing FSRV for high enough frequencies such that the thermal wave component is nearly negligible [compare the 0.1 kHz phase curve and the 5 kHz and 50 kHz phase curves in Fig. 1(b)]. This is so because the higher recombination rate at the surface creates a larger carrier density gradient that results in a higher diffusion rate toward the surface and moves the carrier-density-wave distribution centroid nearer to the surface. This phenomenon, in the absence of any interference from the thermal component signal, leads to saturated phase lags with the signal from more strongly absorbed wavelengths exhibiting smaller phase lags than the deeper penetrating wavelengths. However, for very high surface recombination rates the thermal component of the signal begins to dominate, even at high frequencies that are generally dominated by the carrier wave component, causing an increase in the phase lag [Fig. 1(b)]. The prevalence of the thermal contribution over that of the plasma decreases as the absorption depth of the excitation source increases.

The stronger influence of the front surface on the PTR signal for shorter wavelengths can also be seen in Figs. 2–4. For these frequency-scan simulations, the incident power was assumed constant resulting in a shift of the amplitude curves to higher magnitude as the photon energy decreases and the number of photons, and consequently the number of injected carriers contributing to the depth integral (assuming a quantum yield of one free carrier per absorbed photon), increases. The influence of the photon energy is also exhibited in the low-frequency phase lag and the slope of the low-frequency amplitude curve (Fig. 2). Although these effects are small, the shorter wavelengths do exhibit a steeper slope and a larger phase lag [Fig. 2(c)] at low frequencies than do the longer wavelengths. This is consistent with increasing the thermal contribution with the signal phase centroid dominated by harmonic conduction heat (thermal-wave) transfer to the bulk. The higher-energy photons of the shorter wavelengths release more thermal energy through the intraband thermalization process after they have been absorbed. It should be noted that while the higher reflection coefficient at shorter wavelengths, which has been accounted for in the model, does contribute to the difference in the carrier injection rate, this difference is too small to be the only contributing factor to the separation of amplitude curves seen in Fig. 2. Clearly, the difference in number of photons absorbed, $E = Nh\nu$, is the main source.

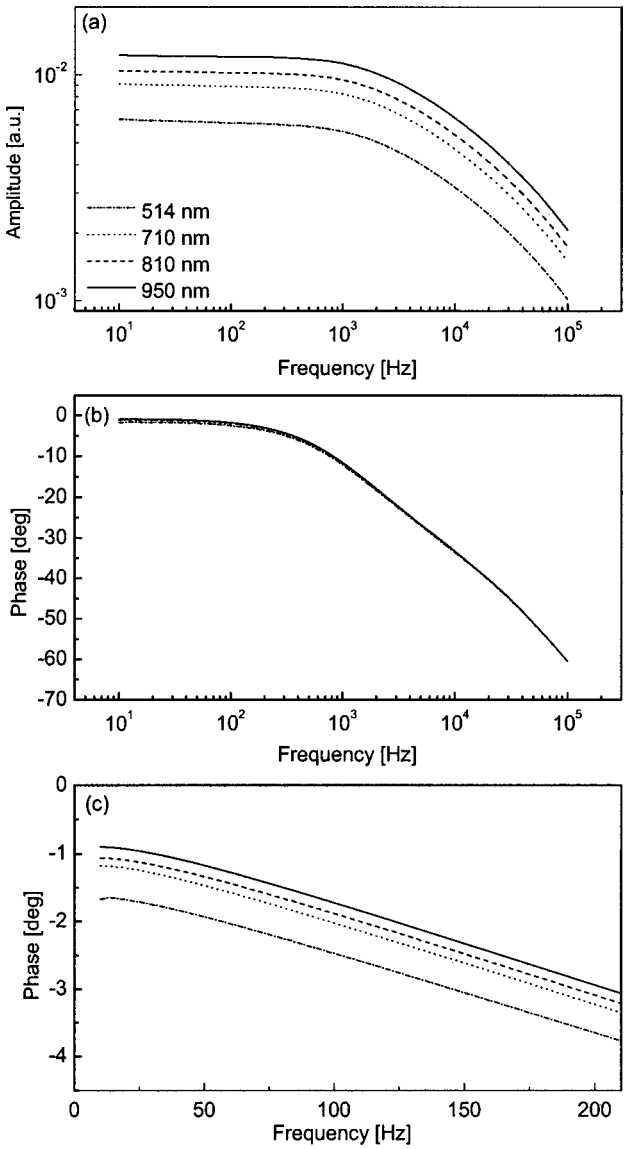

FIG. 2. Amplitude (a) and phase (b) of simulated PTR frequency scans for various excitation wavelengths with FSRV = 0 with a closeup of the low-frequency phase (c).

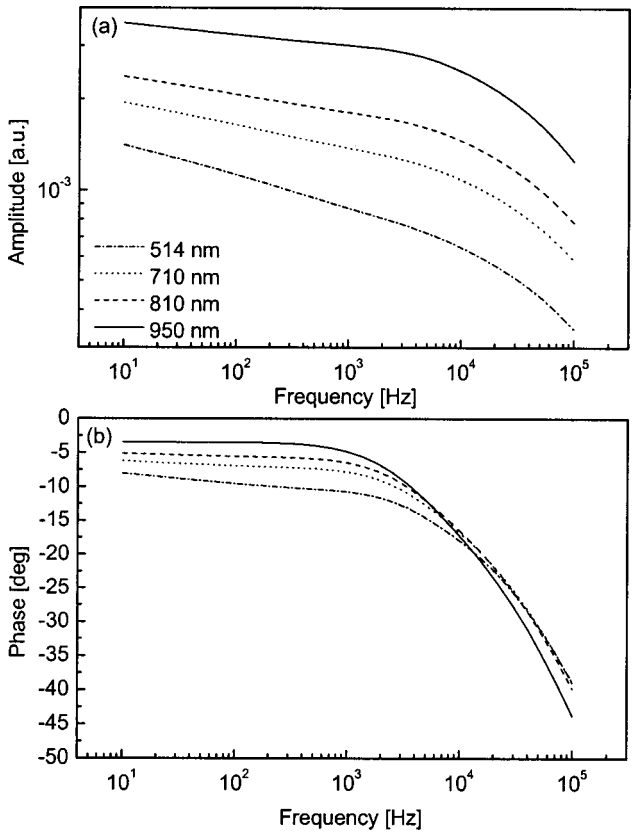

FIG. 3. Amplitude (a) and phase (b) of simulated PTR frequency scans for various excitation wavelengths with FSRV = 10^4 cm/s.

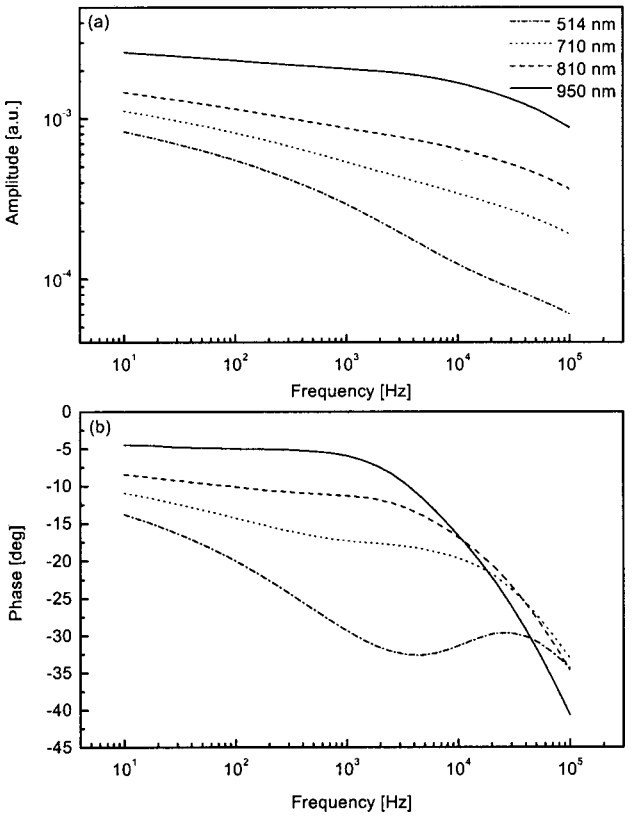

FIG. 4. Amplitude (a) and phase (b) of simulated PTR frequency scans for various excitation wavelengths with FSRV $=10^5$ cm/s.

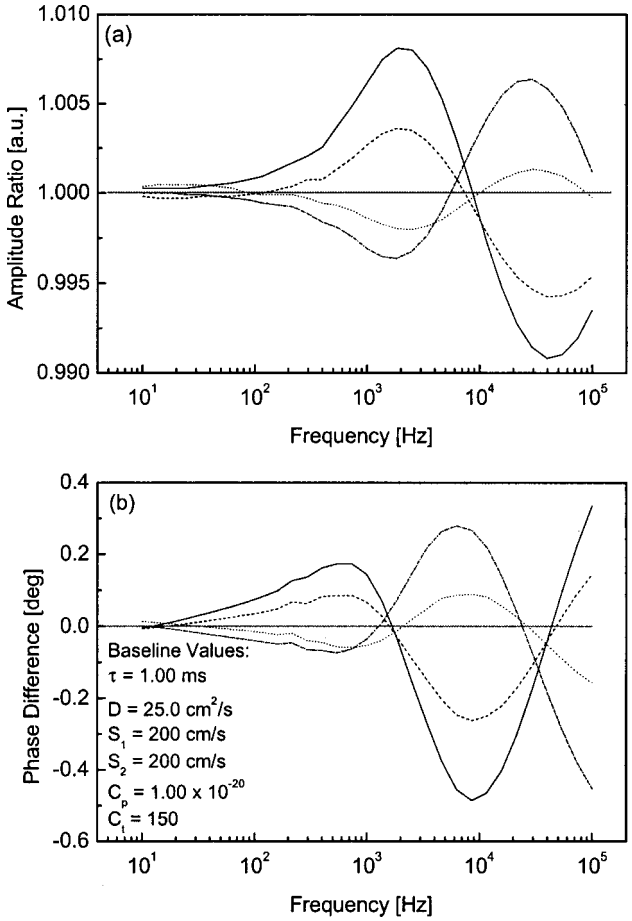

FIG. 5. Amplitude ratio (a) and phase difference (b) between baseline theoretical response and attempted fits to the baseline for fixed changes in the FSRV and no constraints on remaining transport parameters (— $\tau=230$ μs, $D=27.3$ cm^2/s, $S_1=0$ m/s, $S_2=2.0$ m/s, $C_p=1.006\times10^{-20}$, and $C_t=157$; -- $\tau=390$ μs, $D=26.2$ cm^2/s, $S_1=1.0$ m/s, $S_2=2.0$ m/s, $C_p=1.004\times10^{-20}$, and $C_t=154$; · · · · $\tau=3.50$ ms, $D=24.3$ cm^2/s, $S_1=2.0$ m/s, $S_2=2.0$ m/s, $C_p=0.995\times10^{-20}$, and $C_t=146$;— - — - $\tau=5.00$ ms, $D=23.3$ cm^2/s, $S_1=3.0$ m/s, $S_2=1.6$ m/s, $C_p=0.988\times10^{-20}$, and $C_t=146$).

The sensitivity of the PTR signal to the electronic condition of the front surface for several penetration depths is shown in Fig. 3 where $S_1=10^4$ cm/s. It is clearly evident that the FSRV has a greater influence on the PTR response for the shorter wavelengths with shallower optical absorption depths than on the response for the longer wavelengths. As the wavelength and absorption depth decrease, the recombination at the front surface increases leading to a signal that is increasingly dominated by the thermal-wave component—manifested in the increased phase lag and greater slope in the low-frequency region and the diminishing presence of the characteristic ''knee'' in the amplitude curve. For an extremely poor surface with $S_1=10^5$ cm/s (Fig. 4), the PTR response becomes dominated by the thermal signal. However, as the optical penetration depth is increased, the thermal contribution due to the surface recombination becomes less overbearing and the response begins to display the characteristics of a pure carrier-density-wave response. Thus, when attempting to determine the FSRV it is best to use excitation wavelengths with a short absorption depth to increase the signal sensitivity to the surface recombination velocity. On the contrary, when the bulk transport parameters of a semiconductor must be determined, low optical absorption coefficient ranges must be arranged, so as to minimize surface absorption.

It has been shown previously that the parameters of interest for the PTR characterization of a semiconductor (τ, D, S_1, S_2, C_t, and C_p) each have unique influences on the amplitude and phase of the PTR signal.[2] This allows for a unique set of parameter values to be determined by fitting experimental results to the theoretical model. More recent work[14] suggests that for long lifetime samples ($\tau\approx10^{-3}$ s) with high-quality surfaces ($S_1<300$ cm/s) the effects of small variations in the surface recombination velocities on the PTR response are difficult to distinguish from slight changes in recombination lifetime.

In order to investigate the uniqueness of a fit to experiment from a sample meeting these criteria, a set of parameters with a FSRV of 200 cm/s were chosen as a baseline (to simulate an experimental frequency scan) and attempts were made to fit theoretical responses for different FSRVs to this baseline response through the variation of the remaining transport parameters while attempting to maintain the spread of the amplitude and phase from low to high frequency with minimal separation from the baseline at all frequencies. Figure 5 shows the ratio of the simulation to baseline amplitudes and difference in simulation to baseline phases for several values of FSRVs. A decrease in the FSRV can be compensated for by decreasing the lifetime and increasing the diffu-

sion coefficient and an increase in the FSRV can be compensated for by increasing the lifetime and decreasing the diffusion coefficient. It is not possible to achieve a perfect fit to the baseline curve because the knee, slope, and spread of the amplitude and phase curves cannot be identically reproduced with different transport parameters. However, it is possible to compensate for changes in the FSRV (to 100 cm/s and 250 cm/s) and produce a frequency curve with amplitude variation $<1\%$ and phase variation less than 0.2°. Such slight differences are not visible on the scale of the entire frequency scan making it difficult to discern the set of parameters that truly provides the best fit to the experimental data. For this reason, the error between the experiment and the theoretical fit must be calculated to quantitatively determine the quality of the fit.

In order to obtain the best estimate of the transport properties of a material with high-quality surfaces and long lifetime, it is thus necessary to examine the ratio of the amplitudes and the phase difference in a similar manner to that presented in Fig. 5. At approximately 1 kHz, we see that when the FSRV is lower than the baseline, attempts to fit to the baseline result in a knee that occurs at too high a frequency, the higher amplitude at the intermediate frequencies, and a high-frequency slope that is too large. This effect allows the curve to cross back over the baseline and maintain a minimal separation. A similar behavior is exhibited in the phase difference plot. It is also clear that these features become more extreme as the FSRV is further decreased and that an increase in FSRV above the baseline results in similar trends in the opposite directions.

The plots presented in Fig. 5 are for a 950 nm excitation source incident on Si. A similar investigation using 514 nm excitation provided similar trends and values. Although the PTR responses from excitation sources with longer absorption depths in Si show lower sensitivity to the quality of the front surface than the response from the use of more strongly absorbed wavelengths (as discussed herein), at low FSRV, there is little to no spectral dependence on the sensitivity of the PTR signal to changes in the FSRV (see Fig. 1).

IV. CONCLUSION

A three-dimensional theoretical model for the PTR signal from a semiconducting sample excited with a wavelength-scanned laser beam and variable arbitrary optical absorption coefficient has been presented. The effect of a variation of the transport parameters for increasing optical penetration depth has also been discussed.

ACKNOWLEDGMENTS

The authors are grateful to the Natural Sciences and Engineering Research Council of Canada (NSERC) for a Research Grant (for one of the authors, A.M.) and to Materials and Manufacturing Ontario (MMO) for an Enabling Research Contract.

[1] H. Daio, A. Buczkowski, and F. Shimura, J. Electrochem. Soc. **141**, 1590 (1994).
[2] M. E. Rodriguez, A. Mandelis, G. Pan, L. Nicolaides, J. A. Garcia, and Y. Riopel, J. Electrochem. Soc. **147**, 687 (2000).
[3] H. M. Van Driel, in *Semiconductors Probed by Ultrafast Laser Spectroscopy*, edited by R. R. Alfano (Academic, Orlando, 1984), Vol. II, p. 61.
[4] I. N. Bandeira, H. Closs, and C. C. Ghizoni, J. Photoacoust. **1**, 275 (1982).
[5] J. S. Blakemore, *Semiconductor Statistics* (Pergamon, New York, 1962), p. 180.
[6] H. P. Baltes, in *Progress in Optics XIII*, edited by E. Wolf (North–Holland, Amsterdam, 1976).
[7] A. Mandelis, Solid-State Electron. **42**, 1 (1998).
[8] S. J. Sheard, M. G. Somekh, and T. Hiller, Mater. Sci. Eng., B **5**, 101 (1990).
[9] S. J. Sheard and M. G. Somekh, in *Nondestructive Evaluation*, Progress in Photothermal and Photoacoustic Science and Technology vol. 2, edited by A. Mandelis (Prentice–Hall, Englewood Cliffs, NJ, 1994), p. 111.
[10] A. Salnick, A. Mandelis, H. Ruda, and C. Jean, J. Appl. Phys. **82**, 1853 (1997).
[11] J. Batista, A. Mandelis, and D. Shaughnessy, Phys. Rev. B (accepted for publication).
[12] T. Ikari, A. Salnick, and A. Mandelis, J. Appl. Phys. **85**, 7392 (1999).
[13] A. Mandelis, *Diffusion-Wave Fields: Mathematical Methods and Green Functions* (Springer, New York, 2001), Chap. 9.
[14] D. Shaughnessy, M.A. Sc. thesis, University of Toronto, 2002.
[15] D. F. Edwards, in *Handbook of Optical Constants of Solids*, edited by E. D. Palik (Academic, New York, 1998).